HAL
open science

A microfluidic method generating monodispersed microparticles with controllable sizes and mechanical properties

Cheng Zhang, Romain A Grossier, Leda Lacaria, Felix Rico, Nadine A Candoni, Stéphane A Veesler

To cite this version:

Cheng Zhang, Romain A Grossier, Leda Lacaria, Felix Rico, Nadine A Candoni, et al.. A microfluidic method generating monodispersed microparticles with controllable sizes and mechanical properties. 2019. hal-02179400v2

HAL Id: hal-02179400

https://hal.science/hal-02179400v2

Preprint submitted on 3 Sep 2019 (v2), last revised 22 Oct 2019 (v3)

HAL is a multi-disciplinary open access archive for the deposit and dissemination of scientific research documents, whether they are published or not. The documents may come from teaching and research institutions in France or abroad, or from public or private research centers.

L'archive ouverte pluridisciplinaire **HAL**, est destinée au dépôt et à la diffusion de documents scientifiques de niveau recherche, publiés ou non, émanant des établissements d'enseignement et de recherche français ou étrangers, des laboratoires publics ou privés.

Development of a microfluidic method for preparing monodispersed microparticles with controllable sizes and mechanical properties

Cheng Zhang[1], Romain Grossier[1], Leda Lacaria[2], Felix Rico[2], Nadine Candoni[1], Stéphane Veesler[1]

[1]*CNRS, Aix-Marseille Université, CINaM (Centre Interdisciplinaire de Nanosciences de Marseille), Campus de Luminy, Case 913, F-13288 Marseille Cedex 09, France*

[2]*Adhesion and Inflammation Lab (LAI)/INSERM U1067 CNRS UMR 7333, 163, avenue de Luminy, Case 937; 13288 Marseille Cedex 09, France*

Abstract

In this article, we present a microfluidic method for the production of monodispersed hydrogel microparticles of Na-/Ca-alginate with controllable sizes (micrometer range) and mechanical properties without using surfactant. Our ultimate aim is to produce microparticles that mimic red blood cells (RBCs). *Ex situ* gelation is carried out to realize the transformation from Na-alginate to Ca-alginate microparticles. Gelation proves essential to obtaining desirable microparticle properties, such as insolubility in water and RBC-like mechanical properties. For both Na-alginate and Ca-alginate microparticles, a smooth surface and a porous inner structure are observed under a scanning electron microscope. A platform of microgrippers is successfully developed to manipulate the microparticles. The Young's modulus, measured using an atomic force microscope on the surface of Ca-alginate microparticles, is of the same order as that of RBCs. Combined with size control to micrometer range, this confirms the feasibility of using Ca-alginate microparticles to mimic RBCs.

Introduction

Microfluidics has emerged as a powerful technique to form discrete and uniform hydrogel structures at the microscale (<100µm).(Utech et al., 2015) This is because droplet-based microfluidic systems permit generation of discrete and uniform microdroplets which are dispersed in a continuous phase.(Zhang et al., 2015) Each microdroplet can be the site of a gelation reaction forming microparticles.(Håti et al., 2016; Utech et al., 2015; Yamada et al., 2012; Zhang et al., 2007) In this paper, we explore the generation of monodispersed hydrogel microparticles for potential applications in medical and biological fields.(Lee and Mooney, 2012)

Alginate is a well-known biopolymer obtained from brown algae. It has been widely applied in drug delivery and tissue engineering due to its biocompatibility, low toxicity, nonimmunogenicity, relatively low cost, and simple gelation with divalent cations such as Ca^{2+} (covalent cross-linking). Alginate is a linear polysaccharide containing varying amounts of 1,4-linked β-D-Mannuronic acid and α-L-Guluronic acid residues arranged in a block-wise manner along the backbone. The composition and residue sequence vary depending on the source.(Lee and Yuk, 2007) Seeking to control the mechanical and/or swelling properties of alginate gels, researchers have investigated covalent cross-linking with different types of molecules and cross-linking densities.(Ouwerx et al., 1998) The purpose of our study was to produce calibrated and monodispersed microparticles with size (5-10µm) and mechanical properties (E=26±7kPa (Dulińska et al., 2006)) similar to red blood cells (RBCs) for the

validation of a cellular ultrasonic imaging setup(Monchy et al., 2018) to assess the RBC aggregation under *in vivo* and *in situ* flow conditions.
Calcium alginate (Ca-alginate) was chosen for its mechanical properties.(Ouwerx et al., 1998) Alginate forms hydrogel by simple gelation with divalent cations, such as calcium cation (Ca^{2+}). However, direct mixing of a calcium solution with an alginate solution in a microfluidic chip gives rise to instant gelation, likely resulting in clogging and non-uniform microdroplet formation(Utech et al., 2015). To overcome this, other approaches were proposed in the literature to provide calcium (a cross-linker):
(1) dissolution of solid particles: internal gelation when solid particles of calcium carbonate are in the dispersed alginate phase, or external gelation when solid particles of calcium acetate are in the continuous phase(Zhang et al., 2007);
(2) chelation of calcium and its controlled release in the microdroplet via acidification(Utech et al., 2015) or exchange of ligands(Håti et al., 2016);
(3) injection of a buffer to delay gelation, acting as a barrier to delay calcium diffusion(Yamada et al., 2012) but requiring a complicated microfluidic chip with up to 7 inlet channels and with a risk of clogging.
Thus, *in situ* gelation using a microfluidic method remains an issue. To overcome this problem we decide to use a solvent extraction method(Freitas et al., 2005; Rondeau and Cooper-White, 2008; Sugaya et al., 2013). We develop a simple 3-step alginate microparticle synthesis. First, sodium alginate (Na-alginate) microdroplets of the desired size and concentration are produced without using surfactant, knowing that the presence of surfactant has shown to have an effect on the particle morphology(Pittermannová et al., 2016). Second, Na-alginate microparticles are obtained by microdroplet shrinkage via water extraction by dimethyl carbonate (DMC). Third, *ex situ* cross-linking is performed with a calcium chloride ($CaCl_2$) solution, which yields Ca-alginate microparticles. Here, unlike most approaches where particle size is controlled exclusively by channel size(Utech et al., 2015), the final size is controlled by channel diameter, chemical composition of the continuous phase, initial Na-alginate concentration ($\mathbf{C_i}$), ratio (**k**) of flow rates between the continuous phase and the dispersed phase and total flow rate (ϕ_{TOT}) of the two phases.

Materials and methods

Chemical materials

Sodium alginate (I3G80), dimethyl carbonate (ReagentPlus 99%, CAS number 613-38-6,) and calcium chloride (22 317.297) were obtained from Alliance Gums and Industries, SIGMA-ALDRICH and PROLABO, respectively. All of these reagents are used without further purification.

Principle of droplet-based microfluidic system with DMC

A droplet-based microfluidic system is constructed (Fig.1) using commercially available polyether ether ketone (PEEK) junctions and Teflon-like tubing (IDEX Health and Science) with inner diameter (ID) 150µm, initially designed for high-performance liquid chromatography (HPLC) systems. These two materials were previously tested in our group and proved to be compatible with almost all solvents, showing excellent resistance and no solvent evaporation.(Ildefonso et al., 2012)
This droplet-based microfluidic system is used to generate hydrogel microparticles dispersed in a flow of continuous phase. We use an aqueous Na-alginate solution (concentration varying over 3 orders of magnitude from 0.006 to 1wt%) as the dispersed phase and dimethyl

carbonate (DMC) as the continuous phase. Although these two phases are immiscible at room temperature, water still has a low solubility (3wt%) in DMC(Stephenson and Stuart, 1986), which ensures the slow exchange between DMC and water.

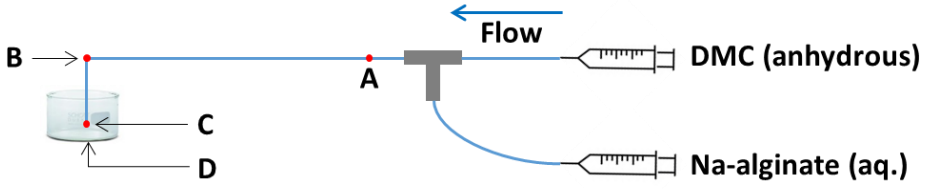

Figure 1: Diagram of the microfluidic setup where **A**, **B, C** and **D** are observation points after microdroplet generation, at the end of the channel, at the outlet of the channel and at the bottom of the collecting vial respectively.

Principle of shrinkage during generation and collection of microdroplets

Our approach is inspired by Rondeau and Cooper-White(Rondeau and Cooper-White, 2008) who studied the formation of biopolymer microparticles using DMC as continuous phase. Along the microfluidic channel, water contained in Na-alginate microdroplets diffuses slowly into carrier fluid DMC (Fig.2). Consequently, the concentration of alginate in the microdroplets increases, assuming negligible diffusion of alginate in DMC.(Rondeau and Cooper-White, 2008) Furthermore, this mechanism implies that the desired microparticle size and concentration can be obtained without using low ID channels or injecting a highly concentrated alginate solution which would be viscous. Note that both of these conditions complicate the procedure, with the risk of blocking microdroplets. Finally, shrunk microdroplets are collected in a DMC-containing vial, where water extraction continues. Because of water extraction by DMC, Na-alginate microdroplets generated in the microfluidic channel shrink, becoming Na-alginate microparticles. After gentle drying at room temperature, alginate cross-linking is realized simply by adding an aqueous $CaCl_2$ solution, forming Ca-alginate microparticles. Figure 3 shows optical micrographs of microdroplets/particles at different observation points during the experiment. It must be pointed out that the method of separation of Na-alginate and Ca-alginate microparticles from solution is a crucial step for potential applications(Pittermannová et al., 2016).

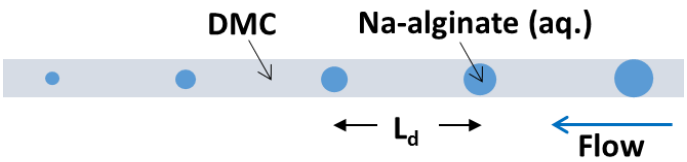

Figure 2: Schematic illustration of the shrinkage of microdroplets in DMC along the microfluidic channel where $\mathbf{L_d}$ is the distance between 2 successive microdroplets.

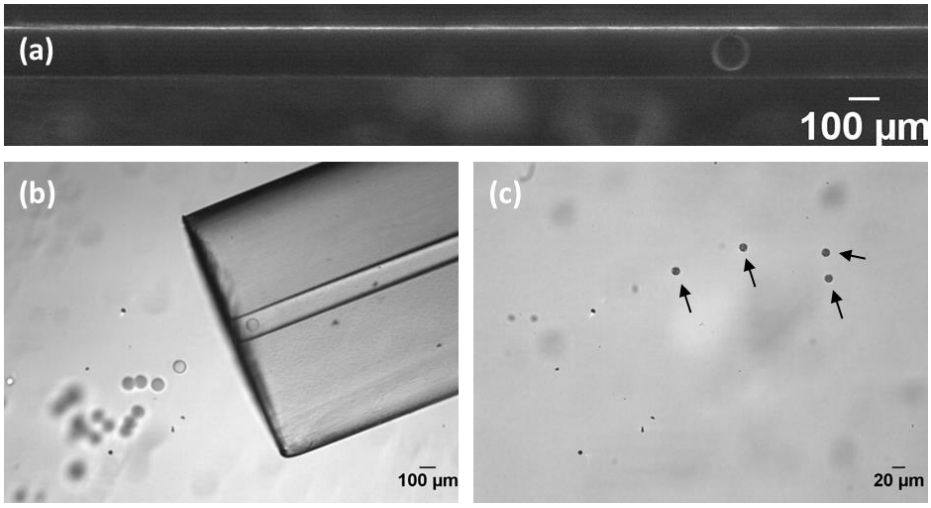

Figure 3: Optical micrographs of Na-alginate microdroplets (**C_i**=0.06wt%) in DMC in a channel (ID 150µm) (a) after generation (point **A** in Fig.1) and (b) at the outlet of the channel (point **C** in Fig.1) during collection in DMC. (c) Na-alginate microparticles (d=11.7µm±1.9%) in DMC, after complete shrinkage, at the bottom of the collecting vial (point **D** in Fig.1).

Characterization of microparticles

- **Scanning electron microscope**

The topology and inner structure of microparticles are observed by scanning electron microscope (SEM, JEOL 6340F), with a low acceleration voltage of 1kV and without coating. After drying at room temperature in air, microparticles are fixed to the bottom of a recipient. They are then transferred to a copper sample plot with carbon tape. This step may break some microparticles, revealing the inner structure. A razor blade is also used to cut microparticles to observe the inner structure.

- **Microgrippers**

The mechanical properties of microparticles are first evaluated using microgrippers (FT-G 102 Force Sensing Microgrippers from FemtoTools). Alginate microparticles, seated in a glass petri dish filled with aqueous solution, are observed with a transmission optical microscope.

- **Atomic force microscope**

The mechanical properties of microparticles are also characterized by measuring the Young's modulus using a NanoWizard atomic force microscope (JPK, Bruker, Santa Barbara, CA, USA). The experiment involves the use of a V-shaped cantilever, an MLCT-Bio-DC(C) (Bruker, Santa Barbara, CA, USA) with a pyramidal probe and a spring constant of 0.01 N/m. Microparticles are deposited on a surface and observed via an inverted optical microscope coupled AFM.

Results and discussion

In-channel microdroplet shrinkage

We discuss here in detail the shrinkage of spherical microdroplets in the microfluidic channel. For each microdroplet, water diffuses both left and right in the channel (Fig.4 (a)). To facilitate the calculation, we consider that water diffuses exclusively in one direction, either left or right (Fig.4 (b)), until DMC is saturated.

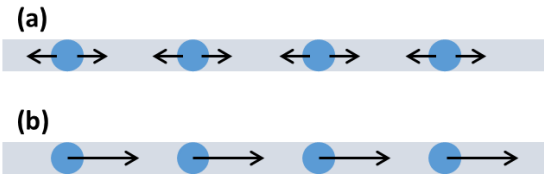

Figure 4: Illustration of water diffusion (a) in reality and (b) for simplified calculation during the extraction by DMC in the channel.

Thus, the quantity of DMC in the volume between two microdroplets ($\mathbf{V_d}$), related to the distance between two microdroplets ($\mathbf{L_d}$), determines the maximum quantity of water that can be extracted from one microdroplet. For a microfluidic channel of inner diameter **d**, $\mathbf{V_d}$ is calculated with the equation (1).

$\mathbf{V_d} = \mathbf{L_d} \times \pi(\mathbf{d}/2)^2$ (1)

Obviously, given the limited solubility (3wt%) of water in DMC, a certain $\mathbf{L_d}$ (or $\mathbf{V_d}$) is required to achieve the desired decrease in diameter (or volume) of microdroplets.

We demonstrate here a method of estimating the required $\mathbf{L_d}$ to obtain a given reduction in diameter after shrinkage of microdroplets of initial diameter $\mathbf{d_i}$. Because the diffusion of Na-alginate in DMC is negligible(Rondeau and Cooper-White, 2008), the decrease in microdroplet diameter (or volume) is only due to the loss of water extracted by DMC. The desired diameter is attained when DMC is saturated by water. This equilibrium state is described by equation (2) indicating that the volume of water diffused to DMC determines the reduction in microdroplet volume $\mathbf{R_v}$(%):

$\mathbf{V_d} \times 3\% = (4/3)\pi(\mathbf{d_i}/2)^3 \times \mathbf{R_v}(\%)$ (2)

As a first approximation, we assume that microdroplets are generated with an initial diameter $\mathbf{d_i}$ close to the channel ID ($\mathbf{d_i} \approx \mathbf{d}$). Then by combining equation (1) and (2), we get equation (3) showing the ratio between required microdroplet distance $\mathbf{L_d}$ and initial microdroplet diameter $\mathbf{d_i}$.

$\mathbf{L_d}/\mathbf{d_i} \approx \frac{2}{9}\mathbf{R_v}$ (3)

As an example, there is a decrease in diameter of 90% from microdroplets with diameter 150µm to microparticles with the same diameter range as RBCs (e.g. 15µm). This corresponds to a decrease in volume $\mathbf{R_v}$ of 99.97%. Therefore, according to the theoretical calculation (3), the ratio $\mathbf{L_d}/\mathbf{d_i}$ required is:

$\mathbf{L_d}/\mathbf{d_i} \approx 22.2$ (4)

Operating parameters required for desired microdroplet diameter

The channel containing microdroplets and DMC is observed at points **A** and **B**, situated at 5cm and 63cm respectively from the outlet of T-junction (Fig.1).

- ***Controlling the distance between microdroplets L_d***

Experiments are conducted to study the generation of microdroplets at point **A**, by varying the flow rates of dispersed phase ϕ_D and continuous phase ϕ_C (Fig.S1 in the supplementary material). ϕ_D is varied from 0.001 to 0.3 µL/s and ϕ_C from 0.01 to 0.6 µL/s. For each pair (ϕ_D and the corresponding ϕ_C), $\mathbf{L_d}$ is measured at point **A**. Each pair corresponds to a given ratio **k** (ϕ_C/ϕ_D). Regarding the total flow rate ϕ_{TOT} ($\phi_D+\phi_C$), our pairs are divided into two groups with low and high values of ϕ_{TOT}. Plotting $\mathbf{L_d}/\mathbf{d_i}$ versus **k** for each range of ϕ_{TOT} (Fig.S2 in the supplementary material) shows an increase in $\mathbf{L_d}/\mathbf{d_i}$ with **k**, with a linear relationship and slope

depending on ϕ_{TOT}. This result is consistent with our previous findings on the influence of ϕ_D/ϕ_C (i.e. **1/k**) and ϕ_{TOT} on microdroplet diameter $\mathbf{d_i}$.(Zhang et al., 2015)
Finally, the fitting equation obtained for each value of ϕ_{TOT} gives the value of **k** required to reach $\mathbf{L_d/d_i}$=22.2 (Eq. (4)), corresponding to a volume reduction of 99.97% (crosses in Fig.S2 in the supplementary material). This means that with a low and a high total flow rate, a value of 21 and 38 for k respectively ensures a volume reduction of 99.97%. Moreover, assuming a maximum reduction of volume $\mathbf{R_v}$<100% for the final microparticle, equation (3) demonstrates that this $\mathbf{R_v}$ is attainable with $\mathbf{L_d/d_i}$<22.3. This is why the fitting curves are stopped at $\mathbf{L_d/d_i}$<22.3. However, loss of water takes time and the microdroplet moves forward in the channel during this time. Therefore, the length of channel required to reach the final diameter depends on flow rates and is discussed below.

- ***Influence of residence time on shrinkage rate***

For a given **k**, microdroplets are observed at points **A** and **B**. Figure 5 shows optical micrographs of microdroplets at point **B** obtained for ϕ_{TOT} varying from 0.1 to 0.2 µL/s, thus between the two ϕ_{TOT} ranges described above (see fitting curves). Because of **k** values (20, 30 and 40), $\mathbf{L_d}$ is too large to be photographed for measurement. Nevertheless, we observed microdroplet shrinkage for all three values of **k**. According to optical micrographs taken at points **A** and **B**, the volume of microdroplet reduces 17%, 71% and 99% respectively for **k** of 20, 30 and 40. Thus, microdroplet shrinkage or water loss increases with **k**. Moreover, the significant shrinkage for **k**=40 is confirmed by observation of microdroplets at different points along the channel (between **A** and **B**) in Figure S3 of the supplementary material. The final diameter of microparticles is about 10µm, which is in the same range as RBCs.
However, assuming $\mathbf{L_d/d_i}$=22.2 (eq. (4)) for $\mathbf{R_v}$ of 99.97%, i.e. a diameter reduction of 90% (crosses in Fig. 5), experiments should lead to a diameter reduction of around 50%, 80% and almost 100% for **k** of 20, 30 and 40, respectively. Obviously, the shrinkage rate at point **B** is lower in reality than that calculated. This is probably due to the insufficient residence time τ of microdroplets in the channel between points **A** and **B,** which limits the loss of water. Moreover, τ decreases with ϕ_{TOT} since the distance between **A** and **B** is fixed. Therefore, we can either increase the channel length or continue the shrinkage by collecting microdroplets in DMC.

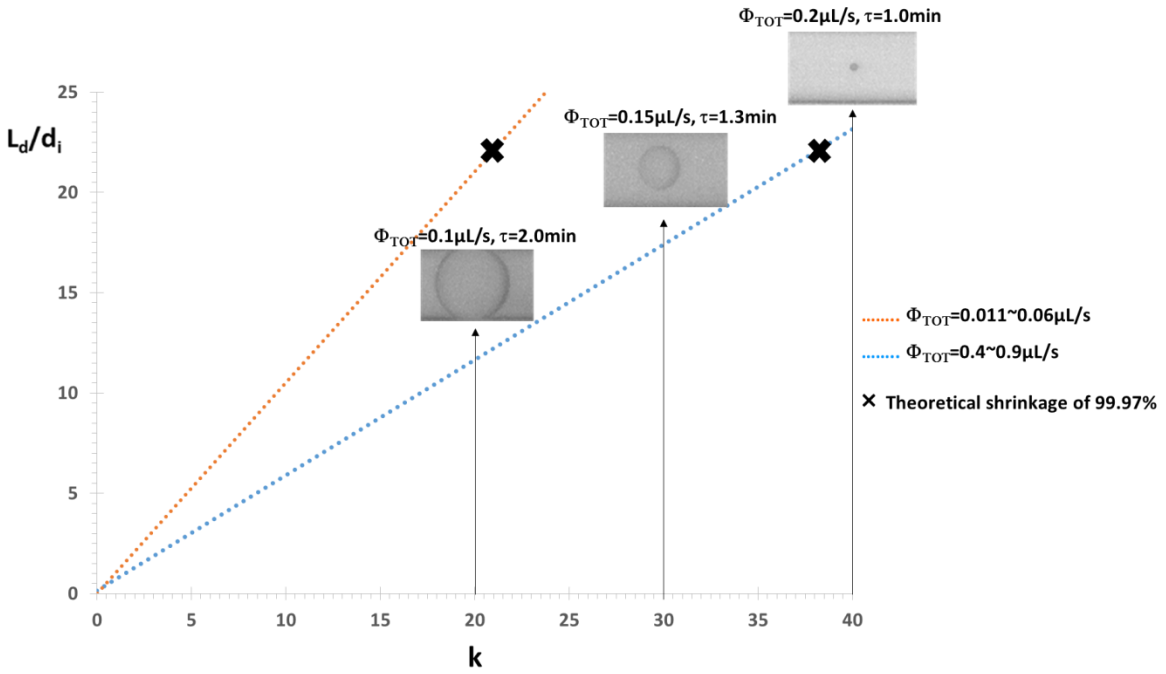

Figure 5: Fitting of $\mathbf{L_d/d_i}$ versus **k** for two range values of ϕ_{TOT} from figure S2 with observations of microdroplets at point **B** (63cm from T-junction outlet, Fig.1) for ϕ_{TOT} from 0.1 to 0.2µL/s. Markers (×) correspond to theoretical shrinkage of 99.97% in microdroplet volume, i.e. 90% diameter reduction ($\mathbf{L_d/d_i}$=22.2). τ: Residence time of microdroplets in the channel. (Initial Na-alginate concentration $\mathbf{C_i}$=0.02wt%, channel length **L**=70cm.)

However, a long channel causes instability of fluids probably because of the pressure drop. For instance, microdroplets at the end of the channel for **k**=40 and ϕ_{TOT}=0.205µL/s are observed to approach each other, forming aggregations because no surfactant is used (Fig S4 of the supplementary material). They flow together towards the outlet, despite the fact that they start out relatively far from each other due to the high value of $\mathbf{L_d}$. Actually, because of shrinkage, when microdroplet diameter becomes too small compared to channel ID, microdroplets can then move towards the inner wall of the channel and may be affected by contamination there. According to our experience, a clean channel is key to avoiding the aggregation of microdroplets. Thus, careful cleaning of the channel with ethanol before experiments is highly recommended, especially when a high **k** is required. Contrastingly, for low values of **k**, the main risk is coalescence of microdroplets when leaving the channel. This can be prevented by gentle hydrodynamic agitation. Thus, in addition to the careful choice of **k**, certain operating techniques are also important in achieving desired microparticle size.

- *Shrinkage during collection:* from microdroplets to microparticles of Na-alginate

When collected in DMC, Na-alginate microdroplets continue to shrink and finally form spherical Na-alginate microparticles. Initial values of microdroplet diameter ($\mathbf{d_i}$) and Na-alginate concentration ($\mathbf{C_i}$) are varied to study their effect on the final values of microparticle diameter ($\mathbf{d_f}$) and concentration ($\mathbf{C_f}$) after collection.

For the experiments in Figure 6, microdroplets of $\mathbf{d_i}$ from 110 to 220µm are generated with $\mathbf{C_i}$ of Na-alginate solutions varying from 0.006 to 1wt%. Figure 6a shows that $\mathbf{d_f}$ increases with both $\mathbf{C_i}$ and $\mathbf{d_i}$. Similar results were previously found for porous microparticles of Na-poly(styrenesulfonate) formed by inkjet injection(Yang et al., 2015). In our study, for each $\mathbf{C_i}$,

$\mathbf{d_f}$ versus $\mathbf{d_i}$ is fitted by a power law. According to the fitting equations, the exponent is about 0.3-0.4 for all $\mathbf{C_i}$, whereas the constant factor increases with $\mathbf{C_i}$ (Fig.6a). Since $\mathbf{d_f}$ does not greatly vary with $\mathbf{d_i}$ when $\mathbf{C_i}$ is fixed, a mean value of $\mathbf{d_f}$ is calculated for each $\mathbf{C_i}$ and plotted versus $\mathbf{C_i}$ (Fig.6b). This leads to another power law dependence. This curve enables the initial concentration of Na-alginate to be defined so as to obtain a given final microparticle size. It is noteworthy that spherical microparticles with a post-collection diameter $\mathbf{d_f}$ of 7.7µm±3.4% are obtained with $\mathbf{C_i}$=0.006wt% (Fig S5 of the supplementary material), indicating that RBC size is attainable using this process.

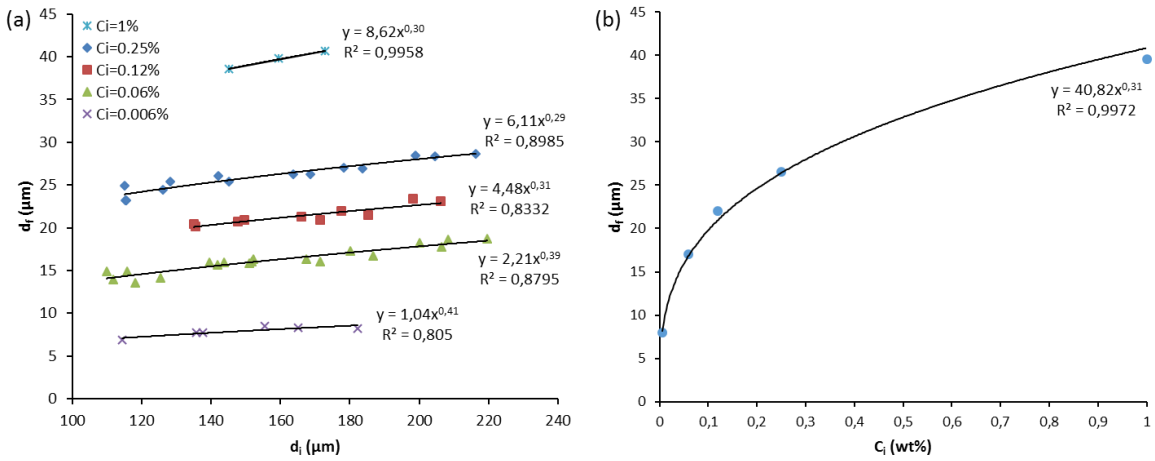

Figure 6: (a) The final microparticle size $\mathbf{d_f}$ as a function of initial microdroplet size $\mathbf{d_i}$ for different Na-alginate concentrations $\mathbf{C_i}$ (0.006 to 1wt%); (b) Plot of the final microparticle mean diameter $\mathbf{d_f}$ after collection versus the initial Na-alginate concentration $\mathbf{C_i}$.

In addition, the final concentration of Na-alginate ($\mathbf{C_f}$) in the microparticle after collection is estimated from initial and final volumes of the microdroplet ($\mathbf{V_i}$ and $\mathbf{V_f}$), considering that the quantity of Na-alginate in the microdroplet remains constant. Therefore, we assume as above that water diffusion from microdroplets to DMC is the only mass transfer. Then $\mathbf{C_f}$ is given by equation (5).

$$\mathbf{C_f}=\mathbf{C_i} \times (\mathbf{d_i}/\mathbf{d_f})^3 \quad (5)$$

From data in Figure 6a and equation (5), $\mathbf{C_f}$ is calculated for different $\mathbf{d_i}$ and $\mathbf{C_i}$ (Figure 7). It is obvious that $\mathbf{C_f}$ depends drastically on $\mathbf{d_i}$, whatever the value of $\mathbf{C_i}$. Thus, a power law fits all the points without distinguishing $\mathbf{C_i}$ values. Note that the fitting equation can be derived from those in Fig.6a (mathematical derivation in supplementary material). This curve enables the initial size of droplets to be defined so as to achieve a given final concentration of Na-alginate in microparticles. This final concentration is important, as it can affect the mechanical properties of the microparticles. Thus, the initial size of droplets controls the final concentration of Na-alginate in microparticles, which in turn may control microparticle mechanical properties.

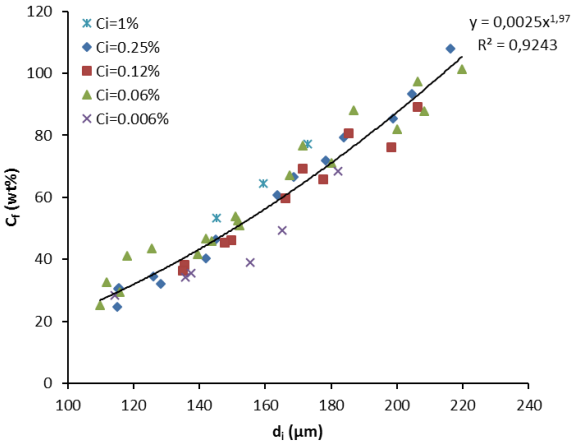

Figure 7: Relationship between the calculated final Na-alginate concentration $\mathbf{C_f}$ in the microparticle and the initial diameter $\mathbf{d_i}$ of droplets with different initial concentrations $\mathbf{C_i}$, with the fitting curve of all data.

From Na-alginate microparticles to Ca-alginate microparticles

All the Na-alginate microparticles are observed to be soluble in water, which limits the chemical composition of media used in further research or applications. Thus, to optimize, we use a divalent cation, Ca^{2+} in our case, for alginate gelation.

- ***Formation of Ca-alginate microparticles by cross-linking with a $CaCl_2$ solution***

After total evaporation of DMC, an aqueous $CaCl_2$ solution is added to the collecting vial containing dried Na-alginate microparticles. The cation of calcium (Ca^{2+}) induces cross-linking (Yang et al., 2015), thus transforming Na-alginate microparticles into Ca-alginate microparticles. Immediate swelling is observed when $CaCl_2$ (0.5%, 1% or 10wt%) is added. The diameter of microparticles increases from 29.5µm±1.1% before cross-linking (dried microparticles obtained with $\mathbf{C_i}$=0.25wt%, **k**=5 and ϕ_{TOT}=0.06µL/s) to 33.5µm±1.5% after immersion and cross-linking (Fig.8 for 0.5wt% of $CaCl_2$). The results are identical whatever the $CaCl_2$ concentration, showing that it has no obvious effect, neither on the shape nor on the size of final Ca-alginate microparticles. Unlike Na-alginate microparticles, all the Ca-alginate microparticles are observed to be insoluble in water. This holds promise for future applications in water.

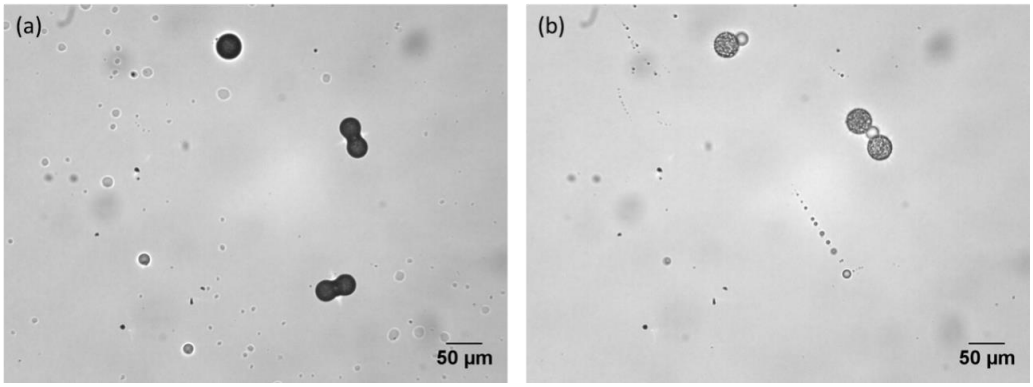

Figure 8: Images of (a) dried Na-alginate microparticles and (b) Ca-alginate microparticles after immersion in $CaCl_2$ solution (0.5wt%). Experimental conditions: $\mathbf{C_i}$ = 0.25wt%, **DMC flowrate**=0.05µl/s and **k**=5.

- ***Characterization of Na-alginate and Ca-alginate microparticles***

In addition to the optical microscope, the scanning electron microscope (SEM) is also used to observe the topology and the inner structure of microparticles. Furthermore, preliminary attempts to characterize microparticle mechanical properties are carried out using microgrippers.

Topology of Na-alginate and Ca-alginate microparticles

SEM images (Fig.9) show that both Na-alginate and Ca-alginate microparticles are spherical with a smooth surface. Ca-alginate microparticles are slightly smaller than Na-alginate microparticles, which seems incompatible with the swelling previously observed (Fig.8). This can be explained by the manipulating conditions under vacuum in SEM. Hence water remaining in the microparticle is extracted and quickly evaporates, causing a second shrinkage after production, until a new equilibrium is reached. This second shrinkage sometimes even causes deformation in the microparticle surface (Fig.S7(b) in the supplementary materials), depending on microparticle properties such as diameter and concentration. This is why, for both Na-alginate and Ca-alginate microparticles, the diameter measured by SEM is smaller than that measured by optical microscope. Moreover, according to SEM measurements, Na-alginate microparticles are larger than corresponding Ca-alginate ones, suggesting that Ca-alginate microparticles lose more water due to the vacuum.

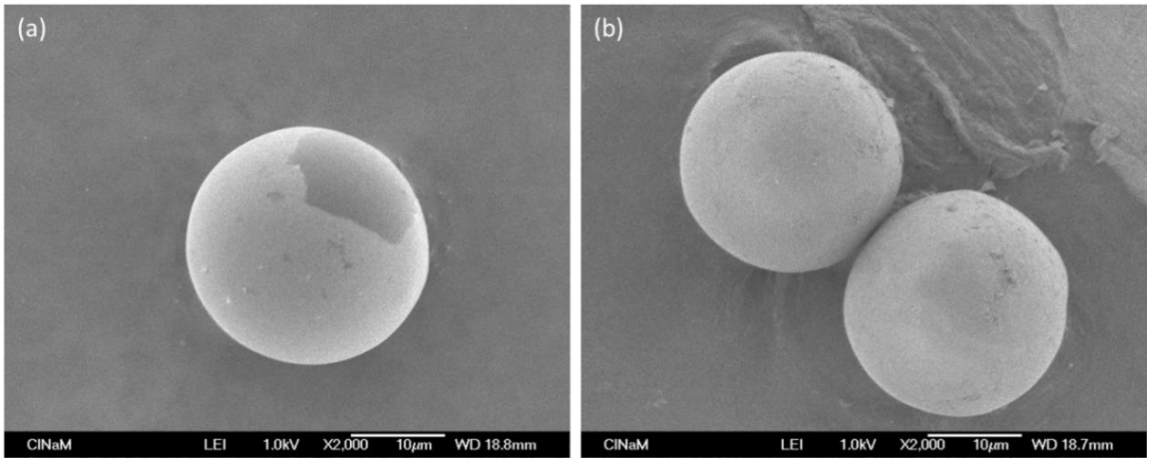

Figure 9: SEM photographs of (a) Na-alginate and (b) Ca-alginate microparticles (formed in a 0.5wt% $CaCl_2$ solution). (Same experimental conditions as for Figure 8)

Inner structure of Na-alginate and Ca-alginate microparticles

Observing a Na-alginate microparticle in DMC under optical microscope (Fig.S6 in the supplementary material) and a dried one under SEM (Fig.10 (a)) reveals a porous inner structure in both cases. Based on this observation, we propose the following mechanism of microparticle formation, in accordance with Yang et al.(Yang et al., 2015) First, after Na-alginate microdroplets are generated, water moves from the microdroplets to DMC. Within the microdroplets, this movement of water also induces the migration of alginate molecules towards the interface with DMC. As a result, 1) an outer shell of alginate forms gradually until it becomes so dense that water can no longer be extracted and therefore remains trapped inside; 2) several inner areas become vacant after the alginate migrates, which explains the observation of pores. Furthermore, the inner structure of Ca-alginate microparticles is also observed to be porous (Fig.10 (b) and Fig.S8), implying that cross-linking by calcium cation does not have an obvious influence on the inner structure of microparticle.

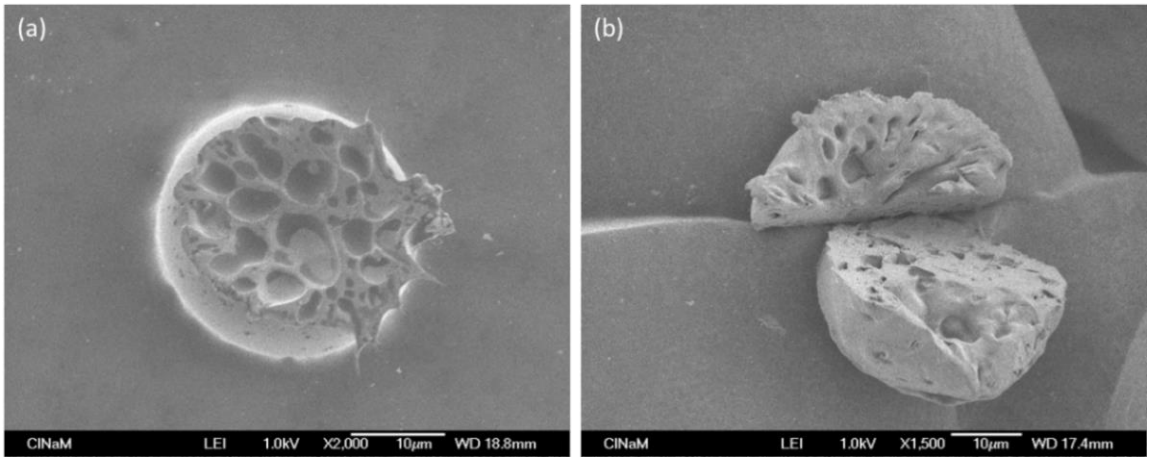

Figure 10: SEM photographs of the inner structure of a (a) Na-alginate and (b) Ca-alginate microparticle (formed in a 0.5wt% $CaCl_2$ solution). (Same experimental conditions as for Figure 8)

Mechanical properties evaluated by microgrippers

After drying, Na-alginate and Ca-alginate microparticles are grasped with force sensing microgrippers to estimate their mechanical properties. Using a 6D positioning system, the microgrippers are placed around the microparticle to be tested. Depending on the voltage supplied to the microgripper left arm (0-170V), the microparticle is grasped and the force sensor of the right arm provides applied force of up to 250µN. This applied force combined with the optical observation gives access to the microparticle reaction to the compression. For the Na-alginate microparticle (Fig.11), we observed (Fig.11 (c)) slipping of the left gripper arm, which indicates a strong resistance to the maximum applied force of 250µN. For both Na-alginate and Ca-alginate microparticles manipulated by microgrippers, no overall deformation was observed.

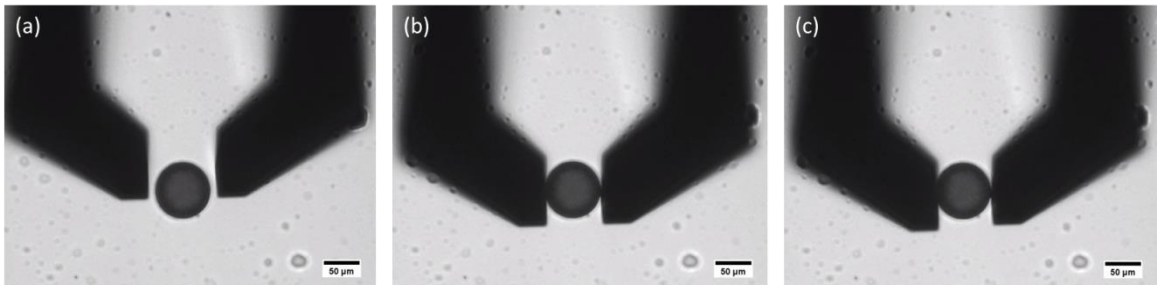

Figure 11: A dried Na-alginate microparticle between microgrippers during (a) approach, (b) contact and (c) force-controlled gripping.

Mechanical properties measured by AFM

The Young's moduli of both Na-alginate and Ca-alginate microparticles are measured by AFM. All measurements are carried out by applying the same force of 0.4nN, an approach velocity of 2µm/s and a z length of 1µm. An 8x8 force curve grid (points separated from each other by 2.5µm) is acquired in the center of the microparticle (Fig.12 (b)). Each point is measured 5 times to obtain 5 force curves/point.

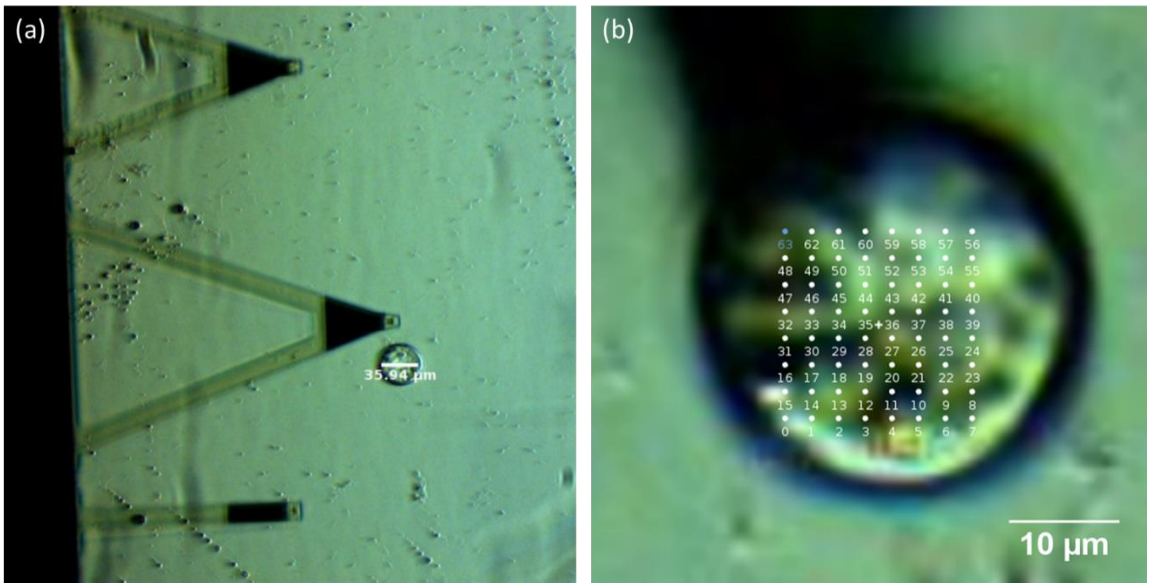

Figure 12: Image of (a) the cantilever used for the force measurement by AFM and a Ca-alginate microparticle in water and (b) an example of a force curve grid on a Ca-alginate microparticle, acquired during the experiment with the inverted optical microscope coupled with AFM.

An example of a force curve is shown in Figure 13. The vertical deflection of the cantilever, proportional to the force, depends on the distance between the AFM probe and the microparticle surface. During measurement, the AFM probe indents about 320nm on the surface (Fig.13), which is less than 1% of the diameter of Ca-alginate microparticles (35µm). Thus, the Young's modulus is measured at the surface of the microparticles.

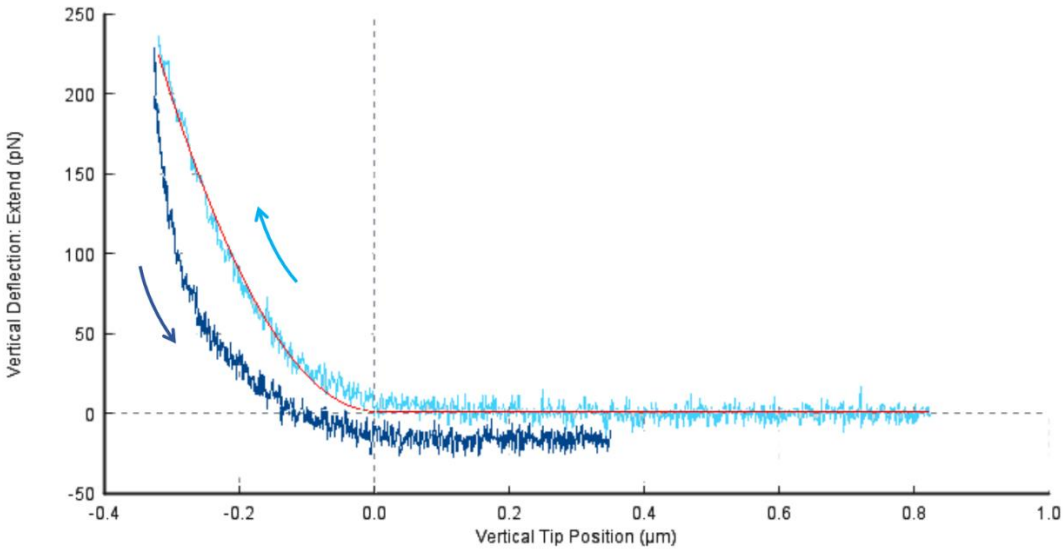

Figure 13: Example of a force curve on a Ca-alginate microparticle: curves relative to cantilever approach and retraction, indicated by arrows, are respectively in light and dark blue; the Hertz Model fit is in red. Zero vertical position shows the point of contact between cantilever and microparticle where no force is applied and the distance between cantilever and sample surface is zero. The negative values of the abscissa, in absolute value, are the indentation, which is the bead surface deformation.

Furthermore, we find that the Young's modulus of Na-alginate microparticles is of the order of MPa, whereas the Young's modulus of Ca-alginate microparticles is 47±43kPa. Obviously, there is a significant decrease in Young's modulus from Na-alginate microparticles to Ca-alginate microparticles. This is due to the swelling observed during the gelation process when

Na-alginate microparticles are immersed in $CaCl_2$ solution. Consequently, Ca-alginate microparticles contain more water than Na-alginate microparticles, reducing the Young's modulus.

Moreover, the Young's modulus of Ca-alginate microparticles (47±43kPa) is of the same order as that of RBCs (26±7kPa), where a similar indentation of 200nm is reported using a similar AFM probe. (Dulińska et al., 2006) It is notable that larger Young's modulus values have been found in pathological RBCs (e.g. 90±20kPa for erythrocytes with G6PD deficiency) (Dulińska et al., 2006) and in RBCs that have undergone specific treatments (e.g. 191±28kPa for formalin-treated cells) (Girasole et al., 2012). Nevertheless, the Young's modulus of Na-alginate microparticles (~MPa) remains beyond the latter range. Gelation is therefore required to effectively produce microparticles with mechanical properties close to those of RBCs.

On the other hand, we also find that the Young's modulus varies substantially depending on the measuring point on the microparticle surface (Fig.S10 in supplementary material). Moreover, this variation also depends on the individual microparticle, even though they are all prepared in the same way from the same experimental batch. This is actually reflected by the relatively high standard deviation in the results (E = 47±43 kPa). Variation in Young's modulus can be due to sample surface irregularities; however, this is not the case here, since the surface of both Na-alginate and Ca-alginate microparticles is smooth according to SEM photographs (Fig.9). Thus, we suggest that the variation may be caused by the microparticles' porous inner structure (Fig. 10 and 14). As shown in Figure 14, the thickness of the shell, defined as the space between the surface and the closest inner pore of the microparticle, varies greatly. Because of the heterogeneity of the porous inner structure, this thickness can be of the same order (500nm) as the indentation of the cantilever probe (320nm), or larger (in µm range). Consequently, it seems that the varying Young's moduli measured can be linked to varying shell thickness. However, further investigations would be required to validate this explanation.

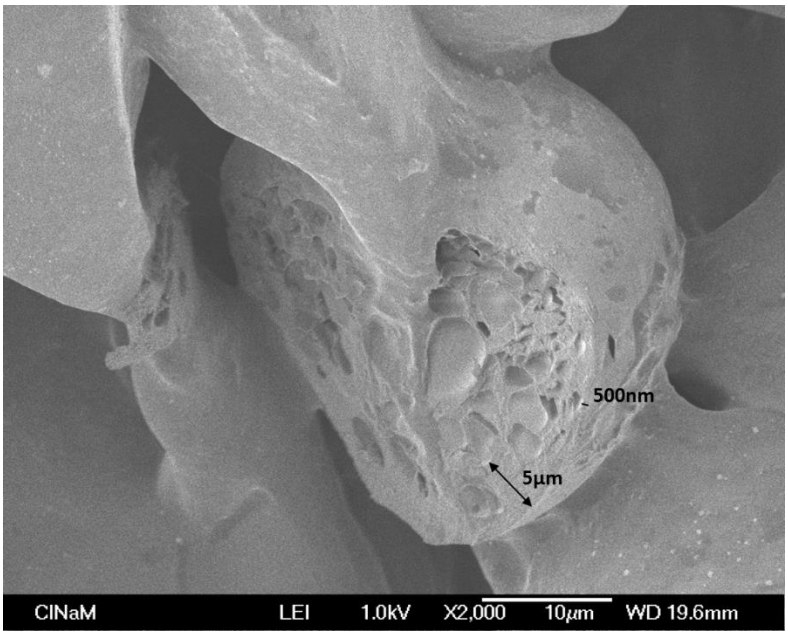

Figure 14: SEM photograph of the inner structure of a Ca-alginate microparticle.

Conclusions and perspectives

In this article, we present a microfluidic method for the production of monodispersed hydrogel microparticles of Na-/Ca-alginate with controllable sizes (micrometer range) and mechanical properties without using surfactant. Our ultimate aim is to produce microparticles that mimic red blood cells (RBCs). *Ex situ* gelation is carried out to realize the transformation from Na-alginate to Ca-alginate microparticles. Gelation proves essential to obtaining desirable microparticle properties, such as insolubility in water and RBC-like mechanical properties. For both Na-alginate and Ca-alginate microparticles, a smooth surface and a porous inner structure are observed under a scanning electron microscope. A platform of microgrippers is successfully developed to manipulate the microparticles. The Young's modulus, measured using an atomic force microscope on the surface of Ca-alginate microparticles, is of the same order as that of RBCs. Combined with size control to micrometer range, this confirms the feasibility of using Ca-alginate microparticles to mimic RBCs and subsequently study the aggregation of RBC under *in vivo* and *in situ* flow conditions with ultrasonic imaging. Moreover, a simple method of separation of Na-alginate and Ca-alginate microparticles from solution is developed for potential application of microparticles, by a gentle drying at room temperature.

Interesting future perspectives include studying parameters such as the concentration of $CaCl_2$ and pH, to determine whether they have an impact on the mechanical properties of Ca-alginate microparticles. This would lead to better understanding and control of microparticle mechanical properties.

Conflicts of interest

There are no conflicts of interest to declare.

Acknowledgements

First, we are grateful to ANR CUMBA (ANR-15-CE19-0017-03) for its financial support of this work. Second, we would like to thank Michel Maton (Alliance Gums and Industries) for his kind provision of sodium alginate. Third, we are also grateful to Mehdi Lagaize for providing technical support for these experiments. Last but not least, we thank Marjorie Sweetko for English revision.

References

Dulińska, I., Targosz, M., Strojny, W., Lekka, M., Czuba, P., Balwierz, W., Szymoński, M., 2006. Stiffness of normal and pathological erythrocytes studied by means of atomic force microscopy. Journal of Biochemical and Biophysical Methods 66, 1-11.

Freitas, S., Merkle, H.P., Gander, B., 2005. Microencapsulation by solvent extraction/evaporation: reviewing the state of the art of microsphere preparation process technology. Journal of Controlled Release 102, 313-332.

Girasole, M., Dinarelli, S., Boumis, G., 2012. Structure and function in native and pathological erythrocytes: A quantitative view from the nanoscale. Micron 43, 1273-1286.

Håti, A.G., Bassett, D.C., Ribe, J.M., Sikorski, P., Weitz, D.A., Stokke, B.T., 2016. Versatile, cell and chip friendly method to gel alginate in microfluidic devices. Lab on a Chip 16, 3718-3727.

Ildefonso, M., Candoni, N., Veesler, S., 2012. A Cheap, Easy Microfluidic Crystallization Device Ensuring Universal Solvent Compatibility. Organic Process Research and Development 16, 556-560.

Lee, K.Y., Mooney, D.J., 2012. Alginate: Properties and biomedical applications. Progress in Polymer Science 37, 106-126.
Lee, K.Y., Yuk, S.H., 2007. Polymeric protein delivery systems. Progress in Polymer Science 32, 669-697.
Monchy, R.d., Rouyer, J., Destrempes, F., Chayer, B., Cloutier, G., Franceschini, E., 2018. Estimation of polydispersity in aggregating red blood cells by quantitative ultrasound backscatter analysis. The Journal of the Acoustical Society of America 143, 2207-2216.
Ouwerx, C., Velings, N., Mestdagh, M.M., Axelos, M.A.V., 1998. Physico-chemical properties and rheology of alginate gel beads formed with various divalent cations. Polymer Gels and Networks 6, 393-408.
Pittermannová, A., Ruberová, Z., Zadražil, A., Bremond, N., Bibette, J., Štěpánek, F., 2016. Microfluidic fabrication of composite hydrogel microparticles in the size range of blood cells. RSC Advances 6, 103532-103540.
Rondeau, E., Cooper-White, J.J., 2008. Biopolymer Microparticle and Nanoparticle Formation within a Microfluidic Device. Langmuir 24, 6937-6945.
Stephenson, R., Stuart, J., 1986. Mutual binary solubilities: water-alcohols and water-esters. Journal of Chemical and Engineering Data 31, 56-70.
Sugaya, S., Yamada, M., Hori, A., Seki, M., 2013. Microfluidic production of single micrometer-sized hydrogel beads utilizing droplet dissolution in a polar solvent, Biomicrofluidics, p. 54120.
Utech, S., Prodanovic, R., Mao, A.S., Ostafe, R., Mooney, D.J., Weitz, D.A., 2015. Microfluidic Generation of Monodisperse, Structurally Homogeneous Alginate Microgels for Cell Encapsulation and 3D Cell Culture. Advanced Healthcare Materials 4, 1628-1633.
Yamada, M., Sugaya, S., Naganuma, Y., Seki, M., 2012. Microfluidic synthesis of chemically and physically anisotropic hydrogel microfibers for guided cell growth and networking. Soft Matter 8, 3122-3130.
Yang, J., Katagiri, D., Mao, S., Zeng, H., Nakajima, H., Uchiyama, K., 2015. Generation of controlled monodisperse porous polymer particles by dipped inkjet injection. RSC Advances 5, 7297-7303.
Zhang, H., Tumarkin, E., Sullan, R.M.A., Walker, G.C., Kumacheva, E., 2007. Exploring Microfluidic Routes to Microgels of Biological Polymers. Macromolecular Rapid Communications 28, 527-538.
Zhang, S., Guivier-Curien, C., Veesler, S., Candoni, N., 2015. Prediction of sizes and frequencies of nanoliter-sized droplets in cylindrical T-junction microfluidics. Chemical Engineering Science 138, 128-139.

Supplementary Material for:

Development of a microfluidic method for preparing monodispersed microparticles with controllable sizes and mechanical properties

Cheng Zhang[1], Romain Grossier[1], Leda Lacaria[2], Felix Rico[2], Nadine Candoni[1], Stéphane Veesler[1]

[1]CNRS, Aix-Marseille Université, CINaM (Centre Interdisciplinaire de Nanosciences de Marseille), Campus de Luminy, Case 913, F-13288 Marseille Cedex 09, France

[2]Adhesion and Inflammation Lab (LAI)/INSERM U1067 CNRS UMR 7333, 163, avenue de Luminy, Case 937; 13288 Marseille Cedex 09, France

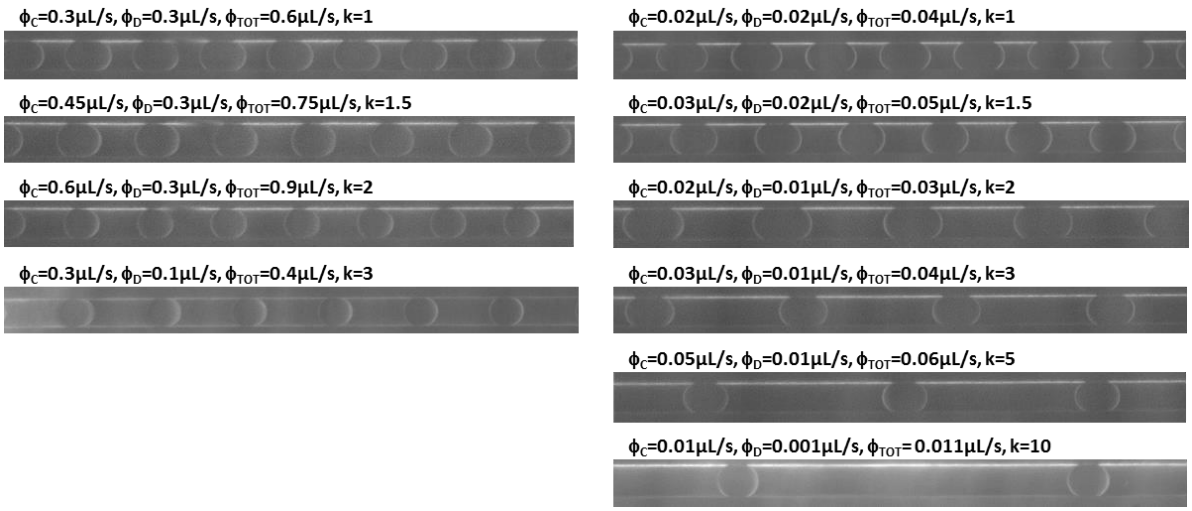

Figure S1: Observation of microdroplets generated in a channel (ID 150µm) under different conditions: flow rates, the ratio of flow rates k between continuous phase and dispersed phase, and total flow rate ϕ_{TOT}.

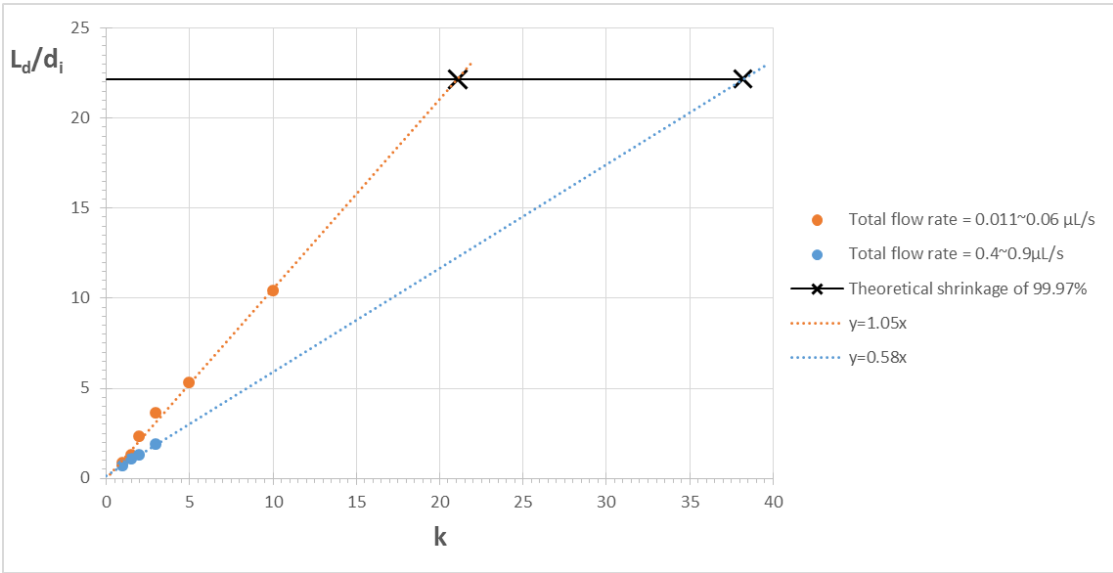

Figure S2: Estimation of L_d/d_i as a function of **k** from Figure S1. Crosses show the theoretical **k** for L_d/d_i=22.2, calculated with eq. (3), to obtain a shrinkage rate of 99.97% in volume for each total flow rate.

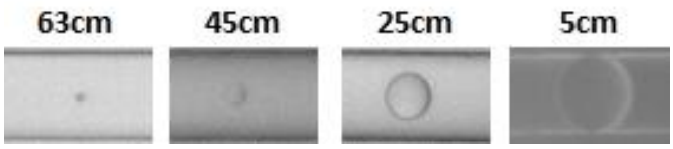

Figure S3: Observation of microdroplet shrinkage at different distances from the T-junction, for the following operational parameters: **k**=40, ϕ_C=0.2µL/s, ϕ_D=0.005µL/s. Channel ID 150µm.

Figure S4: Observation of microdroplets at 63cm from the T-junction, for the following operational parameters: **k**=40, ϕ_C=0.2µL/s, ϕ_D=0.005µL/s. Channel ID 150µm.

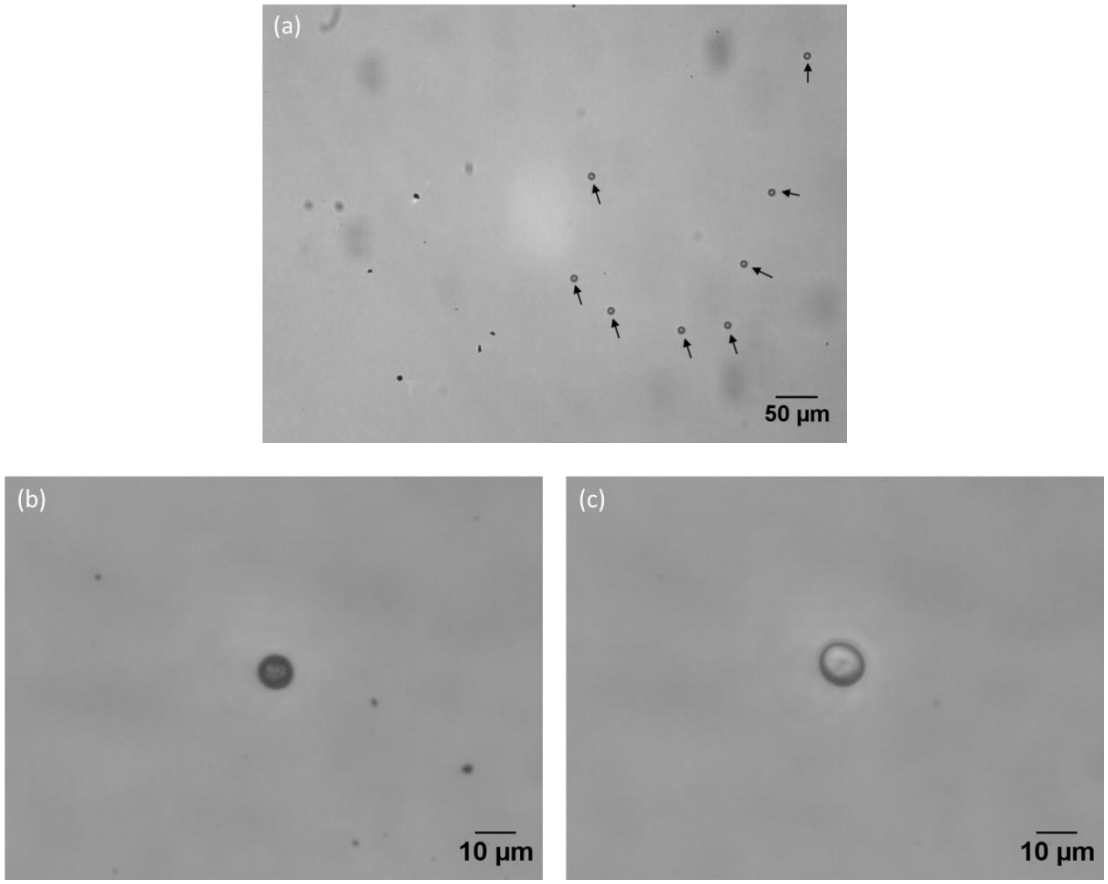

Figure S5: (a) alginate microparticles in DMC; (b) a dried alginate microparticle; (c) the same microparticle as in (b) immersed in $CaCl_2$ (1.35wt%). Experimental conditions: C_i=0.006wt%, DMC flow rate=0.15µL/s, k=30, L=30cm.

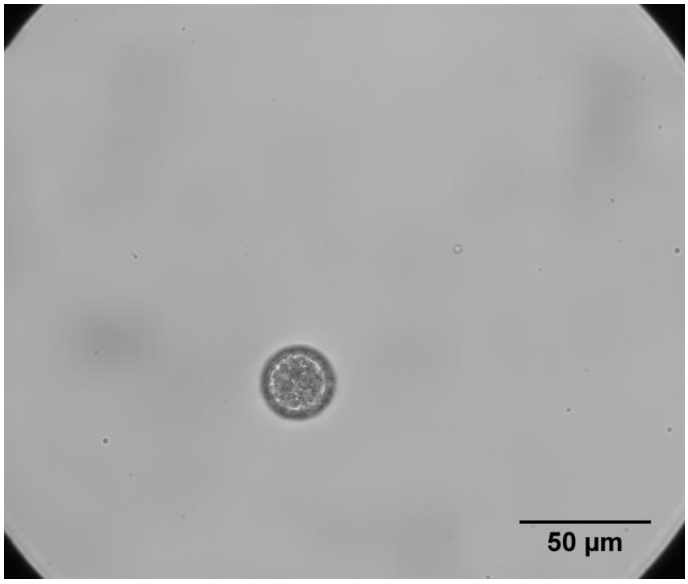

Figure S6: Optical micrograph of Na-alginate microparticle of Fig.8a in suspension in DMC.

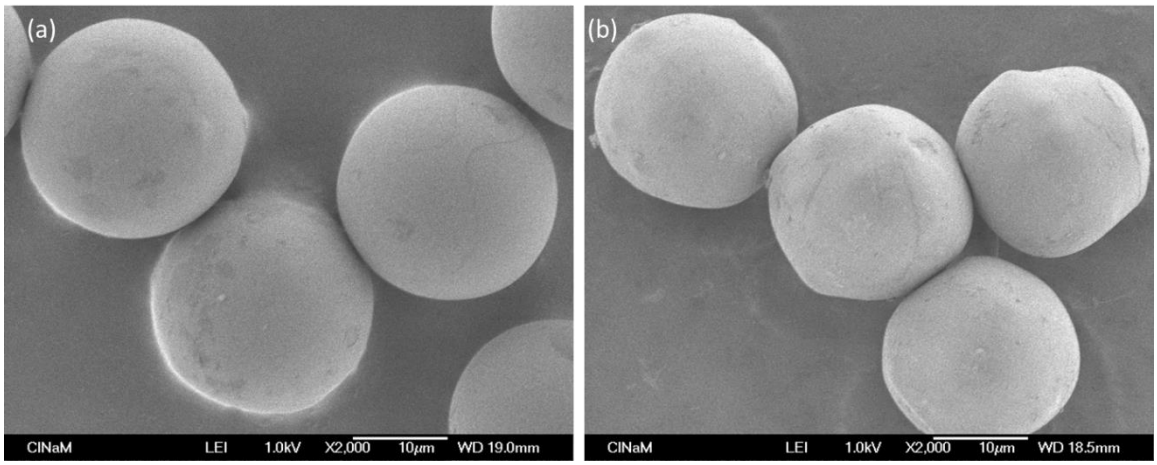

Figure S7: SEM photographs of (a) Na-alginate and (b) Ca-alginate microparticles (formed in a 0.5wt% $CaCl_2$ solution). Experimental conditions: C_i = 0.25wt%, L=19cm, DMC flow rate=0.15µl/s and k=50.

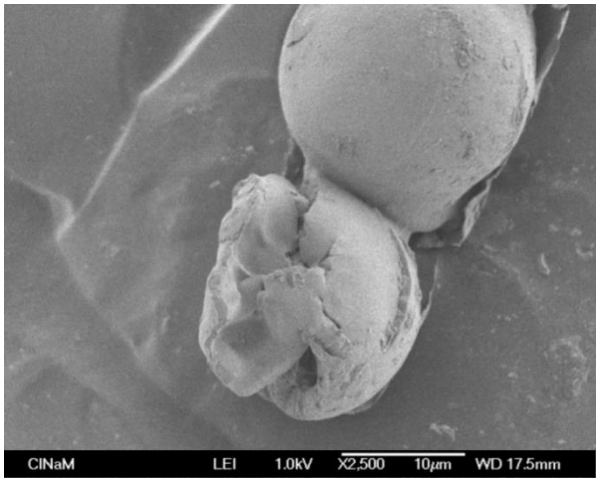

Figure S8: SEM photograph of a squeezed Ca-alginate microparticle (formed in a 0.5wt% CaCl2 solution). (Same experimental conditions as for Figure S7)

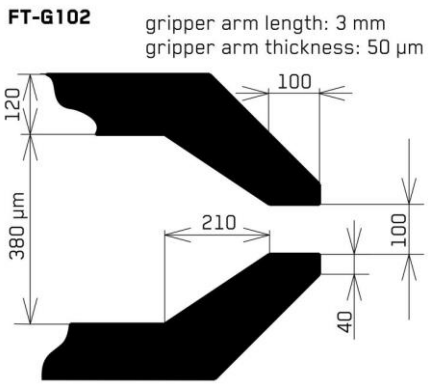

Figure S9: Dimension of the FT-G 102 Force Sensing microgrippers from FemtoTools official site (https://www.femtotools.com/products/ft-mta03/accessories/ft-g-force-sensing-microgripper).

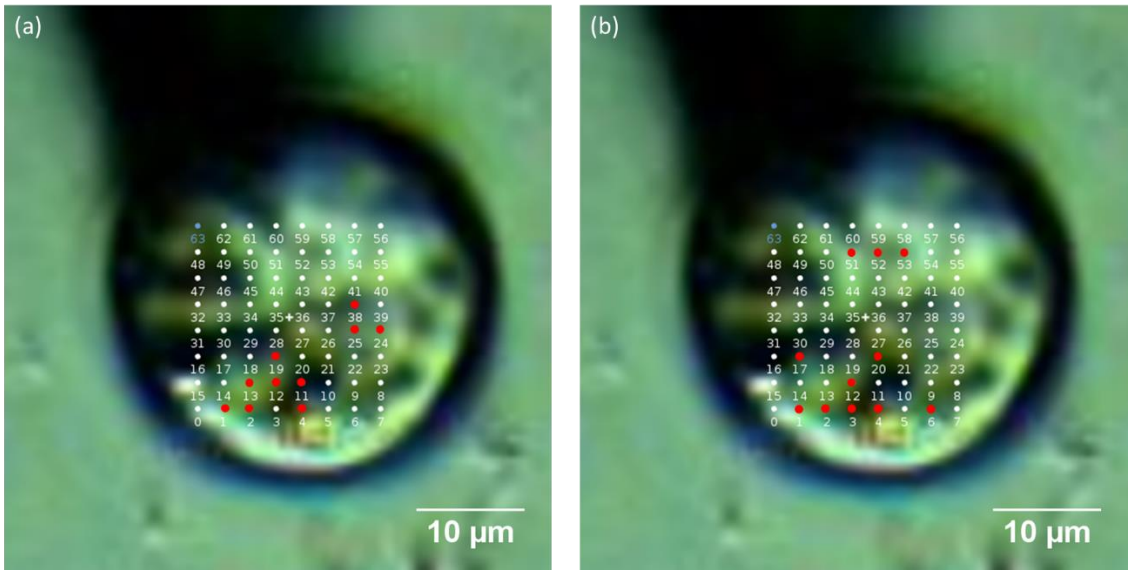

Figure S10: Images of force curve grid on two different Ca-alginate microparticles from the same experimental batch. Red points show the distribution of Young's modulus maxima.

Mathematical derivation of the fitting equation in Figure 7:
From Figure 6a, we have the fitting equation (1) of power law showing d_f as a function of C_i and d_i.

$$d_f = A_{Ci} \times d_i^{\alpha} \quad (1)$$

Here, the constant factor A_{Ci} varies depending on C_i. The exponent α is about 0.3-0.4. We apply it to equation (5) in the article.

$$C_f = C_i \times \left(\frac{d_i}{d_f}\right)^3 = C_i \times \left(\frac{d_i}{A_{Ci} \times d_i^{\alpha}}\right)^3 = \left(\frac{C_i}{A_{Ci}^3}\right) \times d_i^{3-3\alpha} \quad (2)$$

In our experiments, $\left(\frac{C_i}{A_{Ci}^3}\right)$ varies from 0.001 to 0.005 and (3-3α) varies from 1.8 to 2.1.

Consequently, equation (2) corresponds well with the fitting equation shown in Figure 7: $C_f = 0.0025 \times d_i^{1.97}$.